Electronic and Mechanical Modification of Single-Walled Carbon Nanotubes by Binding to Porphyrin Oligomers

Samuel D. Stranks,[†] Johannes K. Sprafke,[‡] Harry L. Anderson,[‡] and Robin J. Nicholas[†,*]

[†]Department of Physics, University of Oxford, Clarendon Laboratory, Parks Road, Oxford, OX1 3PU, U.K. and [‡]Department of Chemistry, University of Oxford, Chemistry Research Laboratory, Oxford, OX1 3TA, U.K.

ABSTRACT We report on the noncovalent binding of conjugated porphyrin oligomers to small diameter single-walled carbon nanotubes (SWNTs) and highlight two remarkable observations. First, the binding of the oligomers to SWNTs is so strong that it induces mechanical strain on the nanotubes in solution. The magnitudes of the strains are comparable to those found in solid-state studies. Comparable strains are not observed in any other SWNT–supramolecular complexes. Second, large decreases in polymer band gap with increasing length of the oligomer lead to the formation of a type-II heterojunction between long chain oligomers and small-diameter nanotubes. This is demonstrated by the observation of enhanced red-shifts for the nanotube interband transitions. These complexes offer considerable promise for photovoltaic devices.

KEYWORDS: carbon nanotube · porphyrin oligomer · type-II heterojunction · strain · photovoltaic

Organic photovoltaics (OPVs) represent a promising route to low-cost solar power. The best results reported to date use donor–acceptor blends which exhibit a type-II heterojunction band alignment to facilitate exciton dissociation at the interface of the blend materials,[1−3] with electron transfer to the acceptor and the hole remaining on the donor. Carbon nanotubes are promising candidates for electron acceptors in these blends owing to their high mobilities and large aspect ratios.[4] In addition, they can be effectively dispersed by donor species such as semiconducting polymers.[4−6] Recently, it has been shown that small-diameter single-walled carbon nanotubes (SWNTs) form a type-II heterojunction with poly-3-hexylthiophene (P3HT)[7,8] and that the blend facilitates ultrafast charge transfer across the interface generating charge transfer states which are long-lived in the presence of excess polymer.[9]

Porphyrins and porphyrinoids are nature's light harvesting system, and they are the primary chromophores in photosynthesis.[10] They have also been proposed as light harvesting components in OPVs. Conjugated porphyrin oligomers are particularly effective at capturing a broad range of the solar spectrum as they have strong absorption bands in both the visible and near-infrared regions. Conjugated porphyrin oligomers also demonstrate high intrachain hole mobilities of 0.1 $cm^2 V^{-1} s^{-1}$ (measured at microwave frequencies)[11,12] comparable to the highest mobility semiconducting polymers such as P3HT.[13] Furthermore, planarized porphyrin oligomers exhibit an order of magnitude increase in intrachain mobility, reaching values of 1 $cm^2 V^{-1} s^{-1}$.

Porphyrins bind strongly to SWNTs due to significant $\pi-\pi$-stacking between the aromatic, planar porphyrin groups and the aromatic nanotube surfaces.[14] Most work has concentrated on monomeric porphyrins[15−18] which are less efficient at harvesting the solar spectrum and have less scope for charge transport. Only a few studies have investigated the binding of oligomeric porphyrins to SWNTs[14,19] including our recent work, where we found that porphyrin oligomers efficiently disperse carbon nanotubes with large binding constants that increase with oligomer length.[20] Generally, the porphyrin oligomers planarize on the SWNTs, and energy transfer processes are observed between the porphyrin and the SWNTs. However, there has been no thorough investigation of the electronic interaction with the carbon nanotubes nor of the energy level alignments.

In this work, we demonstrate that as the porphyrin oligomers increase in length in a SWNT–porphyrin hybrid there is an unusually strong red-shift of the porphyrin $\pi-\pi^*$ absorption bands, due to planarization.

* Address correspondence to r.nicholas1@physics.ox.ac.uk.

Received for review December 24, 2010 and accepted February 14, 2011.

Published online February 28, 2011
10.1021/nn103588h

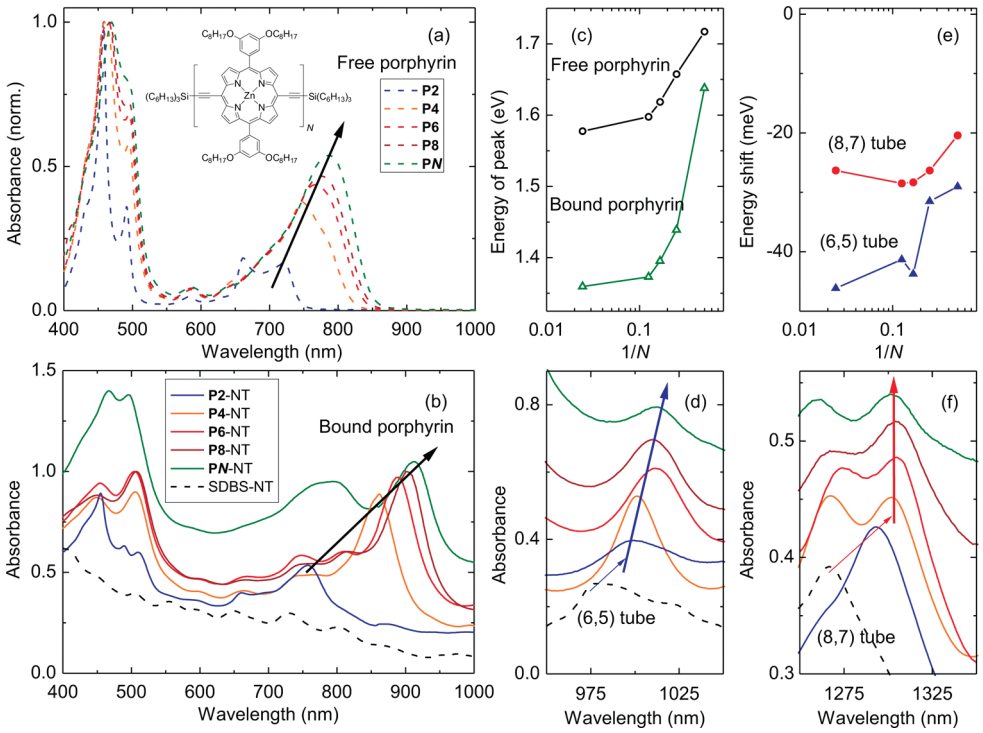

Figure 1. Absorption spectra of the samples under investigation, normalized and offset for clarity. (a) The family of porphyrin oligomers in THF solution. The red-shift of the Q-band with increasing oligomer length is labeled with the black arrow. The inset shows the chemical structure. (b) The porphyrin oligomers when bound to HiPCO nanotubes in THF. The black arrow again shows the red-shift of the Q-band with increasing oligomer length. The black dashed line is the SDBS−HiPCO in D_2O, clearly showing the SWNT E_{22} resonances. (c) Comparing the Q-band porphyrin peak position for the free and bound porphyrin (open circles and triangles, respectively). (d, f) The porphyrin−CoMoCAT and porphyrin−HiPCO composites showing the region of the (6,5) and (8,7) nanotube E_{11} transitions, respectively. The thin arrows highlight the red-shift from the relevant SDBS−SWNT peak (black dashed lines) and the bold arrows show the trend with increasing oligomer length. (e) Comparing the red-shifts for the (6,5) and (8,7) tubes relative to the SDBS samples.

As a result there is a transition from a type-I to a type-II heterojunction which causes an increasing red-shift of the nanotube emission energies. These observations are consistent with the band levels calculated from theory and experiment and show that SWNT−porphyrin oligomer blends would be excellent candidiates for use in OPVs. The porphyrin-SWNT interaction is so strong that it induces mechanical strain in the nanotubes. This changes their band gaps and can be fitted to experimental and theoretical strain models to give a direct measurement of the resulting strain energy.

Carbon nanotubes can be labeled with chiral indices (m,n) which define the nanotube's chiral angle, θ, and diameter, d. The graphene wrapping condition $m - n = 3p + q$ (p is any integer and q is 0, ±1) is used to further classify the nanotubes into metallic ($q = 0$) and the two families of semiconducting nanotubes ($q = \pm 1$). Owing to trigonal warping the two families of semiconducting nanotubes exhibit opposite behavior under mechanical strain, with an increase in the E_{11} transition energy (bandgap) for $q = +1$ and a decrease in E_{11} for $q = -1$ tubes with this behavior reversed for E_{22} transitions.[21,22] This has been demonstrated experimentally for hydrostatic strain,[23] uniaxial strain,[24−26] and combinations of the two,[27] and provides a powerful tool for investigating the magnitudes of the strain components.[22]

RESULTS AND DISCUSSION

We have functionalized carbon nanotubes in tetrahydrofuran (THF) with porphyrin dimers **P2** (N = 2), tetramers **P4** (N = 4), hexamers **P6** (N = 6), octamers **P8** (N = 8) and polymers **P***N* ($N \approx 40$) by sonication and filtration as described in our previous work.[20] Here we use mixtures of carbon nanotubes with either predominantly smaller diameter (CoMoCAT) or larger diameter nanotubes (HiPCO). Nanotubes dispersed in D_2O with the surfactant sodium dodecylbenzene sulfonate (SDBS) were also prepared to provide nanotube controls containing no porphyrin.

Figure 1a shows the absorption spectra of the family of oligomers **P2**−**P***N* in THF. The two primary bands observed are the split Soret band (400−550 nm) and the Q-band (650−850 nm) which corresponds to transitions along the polymer length.[28] With increasing oligomer length, the higher energy component of the Soret band remains unchanged while the lower energy component increases in intensity but no shift in either peak position is observed.[29] The Q-band represents an averaged ensemble of the combinations of configurations of porphyrin units at various torsion angles.[29] The higher energy Q-band also remains unchanged while the lower energy Q-bands, which reflect the highest

occupied molecular orbital (HOMO) and lowest unoccupied molecular orbital (LUMO) levels, significantly red-shift with increasing oligomer length due to increasing conjugation along the polymer axis.[30]

The absorption spectra of the HiPCO−oligomer composites in the region of the bound porphyrin are shown in Figure 1b. Some weak nanotube E_{22} peaks are also present as can be seen from the SDBS−SWNT spectrum (dashed line). Figure 1c shows the lowest energy Q-band porphyrin peak positions found in panels a and b. The free porphyrin shows the well-known red-shift of up to ~140 meV[29,31] with increasing length. For the NT-bound porphyrin the shifts are even larger, with a difference from free to bound polymer of up to ~200 meV and a change with length of up to ~300 meV from **P2** to the polymer **P***N*. This is primarily attributed to increased conjugation along the length of the oligomer[32] owing to planarization[14] of the porphyrin oligomers upon binding to the SWNTs. Any environmental contribution to this red-shift is estimated to be of order 20−30 meV, by comparison with the reduction in nanotube exciton binding energies.[8] A similar planarization of monomer units has been observed recently when P3HT polymers attach to nanotubes, and it has been proposed that such a planar configuration may improve charge transfer between the materials.[33] The absolute shifts are even larger than observed in porphyrin oligomers in double-stranded ladder complexes, or when bound to radial oligopyridine templates, where typical red-shifts relative to the free polymer are of order ~80 meV.[29,31] This suggests that the planarization is significantly more effective when binding to nanotubes. The entire absorption spectra of both HiPCO and CoMoCAT composites are presented in the Supporting Information (Figure S1).

Figure 1d shows the absorption spectra of CoMoCAT−oligomer composites in the region of the small diameter (6,5) E_{11} transition. It is clear that there is a large red-shift of the (6,5) peak position relative to the SDBS−CoMoCAT sample. Importantly, the red-shift increases as the oligomer length progresses from **P2** to **P***N*. This strong oligomer length dependence is not, however, observed for larger diameter nanotubes such as (8,7), as shown in Figure 1f for the HiPCO−oligomer samples. The energy shifts are summarized in Figure 1e, where the length dependence and larger red-shifts are clear for the smaller diameter (6,5) tubes.

These results demonstrate a strong perturbation of both SWNT and porphyrin energy levels in the composites. We understand these findings by comparing the HOMO and LUMO levels of each bound oligomer with the valence (VB) and conduction bands (CB) of the nanotubes in Figure 2. HOMO and LUMO levels of the free oligomers were calculated from the oxidation and reduction potential data of Winters *et al.*[34] using the theory by D'Andrade *et al.*[35] The exciton binding energy was subtracted from these values to match

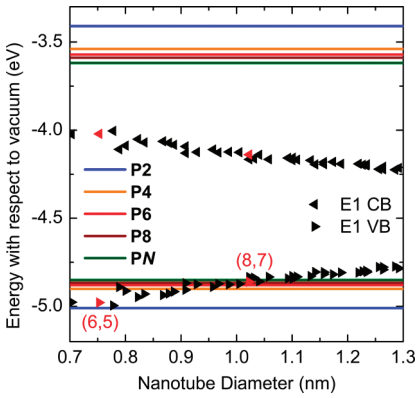

Figure 2. Horizontal lines represent HOMO and LUMO levels of the porphyrin oligomers, with values calculated as discussed in the text. The right and left triangles show the SWNT valence and conduction bands, respectively, plotted as a function of nanotube diameter. The (6,5) and (8,7) tubes are labeled for clarity.

singlet transition energies[36] (see Supporting Information). The red-shift observed upon binding to nanotubes was accounted for by subtracting evenly from the HOMO and LUMO levels, giving a reasonable approximation to the bound porphyrin oligomer levels. Nanotube energy levels were taken from Schuettfort *et al.*[8]

It is clear that, for the smaller diameter tubes (<0.9 nm), a type-II heterojunction is expected to form between all porphyrin oligomers longer than **P2** and the SWNTs. The band overlap becomes larger for longer oligomers and it follows that effects resulting from this type-II interface will be most pronounced for the smallest tubes and the longest oligomers.

This staggered alignment is similar to that at a P3HT−SWNT interface[7] and, therefore, we would expect a similar diameter dependence of the SWNT red-shifts to those observed by Schuettfort *et al.*[8] The red-shifts are attributed to a charge-transfer interaction where the wave function of a hole on the nanotube extends onto the porphyrin oligomer owing to their staggered band alignments, influencing the final exciton transition energy. This acts to raise the effective energy level of the hole and leads to a red-shift of the recombining nanotube exciton. This is only possible for a type-II heterojunction and the effect is more significant for larger band gap (*i.e.*, smaller diameter) tubes where the offset between the oligomer HOMO and SWNT VB is larger. A further consequence of this is that the charge transfer may also be contributing to the red-shift of the porphyrin oligomers, in which case this will primarily influence the HOMO level and lead to an even more pronounced type-II alignment.

To carry out a more quantitative analysis, photoluminescence excitation (PLE) maps of the solutions were taken. Figure 3a,c show the SDBS−SWNT maps for the smaller diameter CoMoCAT and larger diameter HiPCO materials, respectively, and the corresponding

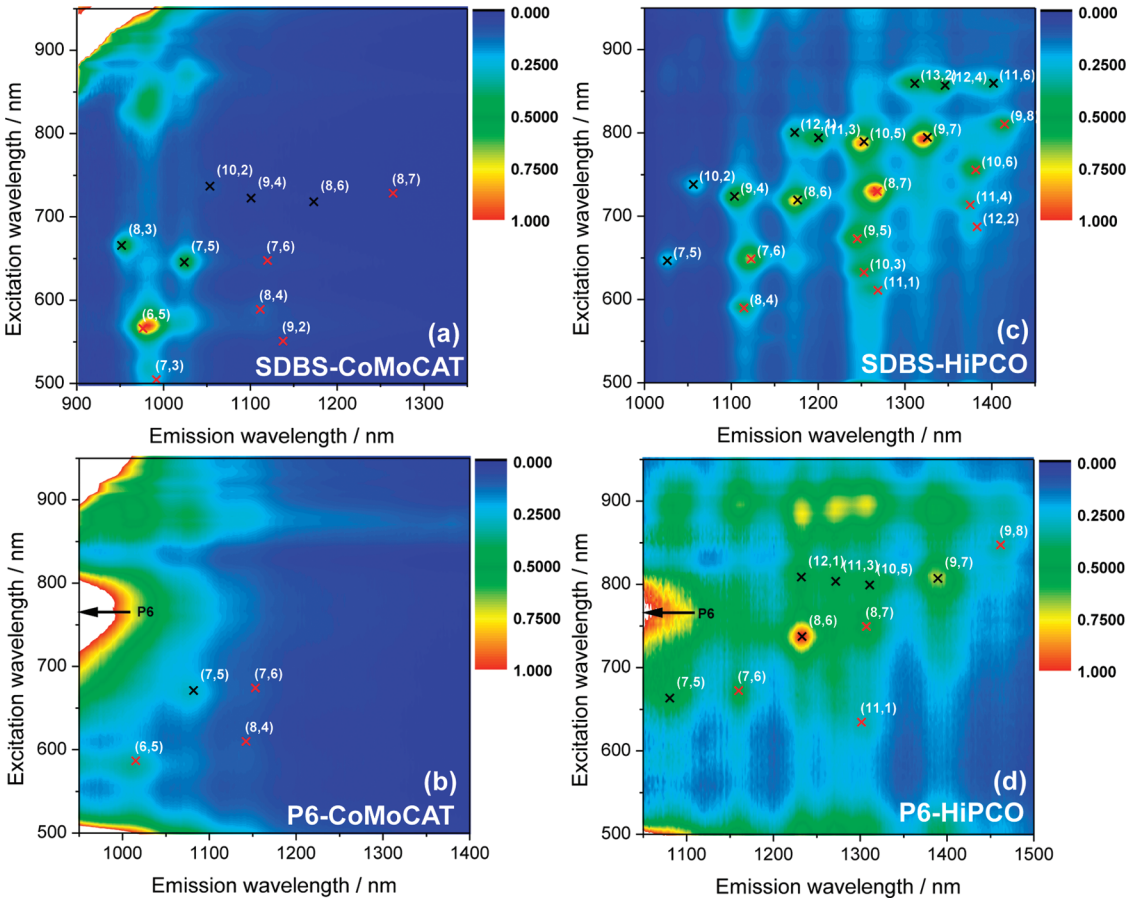

Figure 3. PLE maps of (a) SDBS−CoMoCAT in D_2O, (b) P6−CoMoCAT in THF, (c) SDBS−HiPCO in D_2O, and (d) P6−HiPCO in THF. To emphasize the red-shifts, THF solution abscissa in panels b and d are transposed by 50 nm and the emission tails corresponding to excess porphyrin in these maps are labeled with black arrows. Transition wavelengths for type +1 (−1) nanotubes are labeled with red (black) crosses. Cross-peaks appear in the corners of panels a and d from the excitation source.

maps with the **P6** oligomer are shown in Figure 3b,d. The peak positions were deduced from the maps by fitting with Lorentzian curves[8] and care was taken to account for any excess porphyrin emission tail, while the SDBS−SWNT peaks are labeled according to the values and assignments reported by Weisman *et al.*[37] The horizontal scales for the porphyrin maps are transposed by 50 nm to allow the family behavior to be compared, as a result of the large red-shift of the nanotube transitions upon binding with the porphyrin. In addition, nonselective nanotube emission is observed upon excitation of the porphyrin in either the Soret (∼500 nm) or Q-bands (∼850−900 nm). This corresponds to energy transfer from the porphyrin to the nanotube and has been seen in other nanotube−porphyrin systems.[16,17,20] Finally, the emission intensity of each tube when weighted with tube absorption is greater for the larger chiral angle tubes and the $q = -1$ family due to the dependence of PL quantum efficiencies on chirality and family.[38,39]

SWNT−porphyrin maps with **P2**, **P4**, **P8**, and **P***N* are presented in the Supporting Information (Figures S3 and S4) and similar phenomena are observed. The **P2**−CoMoCAT and both **P***N* maps are dominated by emission from the excess porphyrin which is required for stability, due to its higher quantum efficiency.[40] Nevertheless, significant energy transfer peaks are observed in the **P***N*−HiPCO map, indicating that SWNTs are dispersed by all oligomers. **P4** and **P6**−SWNT maps show the most well resolved peaks, indicating the most efficient dispersions.

To quantify the red-shifts from the PLE maps, we carry out a similar analysis to Schuettfort *et al.*[8] where we consider the red-shifts relative to the values fitted by Weisman *et al.*[37] for sodium dodecyl sulfate (SDS)−SWNT species such that

$$\Delta E_{ii} = E_{ii} - E_{ii}^{\text{Weisman}} \quad (1)$$

Figure 4 shows the NT red-shifts in both E_{11} and E_{22} for the **P6**−SWNT composites. It is clear from this plot that the two NT families exhibit significantly different behavior; for the $q = +1$ tubes, the red-shifts in E_{22} exceed the shifts in E_{11}, but the opposite behavior is observed for $q = -1$ tubes. In addition this difference becomes larger as the chiral angle becomes smaller ($m \gg n$). This behavior is consistent with the presence of a large contribution from mechanical strain effects as described below.

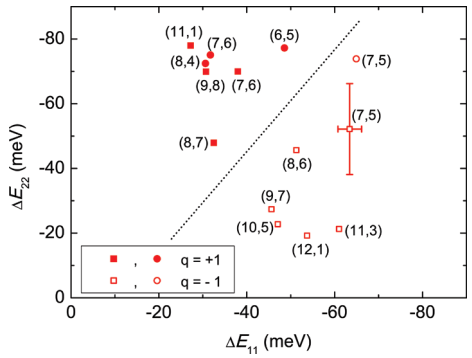

Figure 4. Red-shifts in E_{11} and E_{22} transitions relative to the Weisman values[37] as determined from PLE maps of P6−SWNT composites (Figure 3). The dotted line is a guide to the eye to highlight the different behavior of each family. Circular symbol points are obtained from the CoMoCAT map, square symbols from the HiPCO map and shifts for the (7,5) and (7,6) tubes are obtained from both data sets. A representative error bar is shown, estimated from the instrument resolution and errors in peak fitting.

Similar plots for **P2**, **P4**, and **P8** are presented in the Supporting Information (Figure S5) and exhibit a similar family dependent behavior with an increasing mean red-shift as the oligomer is increased from **P2** to **P8**. It should also be noted that the E_{11} emission energies agree well with the values observed for E_{11} in absorption, indicating that no significant Stokes shifts due to exciton localization are present.

The very close type-II alignment deduced from Figure 2 resembles that observed by Schuettfort *et al.*[8] for P3HT−SWNT composites. As such, we should expect a similar diameter dependence of the red-shift. This was shown to be qualitatively true from absorption measurements (Figure 1) but the red-shifts obtained from PLE maps (Figure 3) show that we need to include strain in addition to any electronic effects from the type-II alignment and the environment. Therefore, we write the two contributions to the total red-shift on a given transition, ΔE_{ii}, as

$$\Delta E_{ii} = \Delta E_{\text{electronic}} + \Delta E_{\text{strain}} \qquad (2)$$

where $\Delta E_{\text{electronic}}$ is the red-shift contribution from the polymer and environment which has previously been shown to be the same for E_{11} and E_{22} to within experimental error.[8] The environment component of $\Delta E_{\text{electronic}}$ (*eg.* dielectric or solvent effects) is of order 20−30 meV and independent of nanotube diameter and oligomer length.[8] The contribution ΔE_{strain} is the red-shift induced by mechanical strain on the nanotubes (positive about $\Delta E_{\text{electronic}}$ for $q = +1$, $i = 1$ and $q = -1$, $i = 2$; negative for $q = -1$, $i = 1$ and $q = +1$, $i = 2$). Since the strain contributions to the E_{11} and E_{22} red-shifts are of opposite signs and are close to equal magnitude, the $\Delta E_{\text{electronic}}$ component is taken as $(\Delta E_{11} + \Delta E_{22})/2$ using the data shown in Figure 4. The ΔE_{strain} component is then given by half of the difference of the E_{11} and E_{22} shifts.

The $\Delta E_{\text{electronic}}$ components of the SWNT red-shifts are plotted as a function of diameter in Figure 5a for the **P6** oligomer. A clear diameter dependence is observed, with a monotonically increasing red-shift as the SWNT diameter is decreased. The trend of the red-shifts is similar to the data for P3HT−SWNT composites found by Schuettfort *et al.*[8] which are also plotted in Figure 5a, and the magnitudes are slightly larger. For further comparison, data taken using a polymer with a known type-I alignment with all SWNT species (poly(2-methoxy-5-(2-ethylhexyloxy)-1,4-phenylenevinylene, MEHPPV) are also plotted and clearly exhibit much smaller shifts and no diameter dependence, as expected. Furthermore, no diameter dependence is observed for any other type-I polymers investigated, namely poly(9,9-dioctylfluorenyl) (PFO), poly(9,9′-dioctylfluorene-*co*-bis-*N*,*N*′-(4-butylphenyl)-bis-*N*,*N*′-phenyl-1,4-phenylenediamine) (PFB) and poly(indenofluorene) (PIF)[8] (data not shown), where all the red-shifts can be accounted for by simple dielectric effects in the polymer which reduce the magnitude of the Coulomb interactions.[41] Finally, no strain effects were observed for SWNT composites with any polymer we investigated, as discussed later in this report. As such, all red-shifts observed for these polymers are electronic effects alone, however data are plotted as $(\Delta E_{11}+\Delta E_{22})/2$ to allow direct comparison with the SWNT−porphyrin data.

Figure 5b shows the $\Delta E_{\text{electronic}}$ components as a function of SWNT diameter for the family of oligomers **P2**−**P8**. The shifts increase with oligomer length and develop a strong diameter dependence for **P6** and **P8**, perhaps an intermediate dependence for **P4**, and a negligible dependence for **P2**. This is entirely consistent with the band alignments and interpretation presented in Figure 2 where a clear type-II heterojunction is established only for the longest oligomers and smallest diameter SWNTs. For **P2**−SWNT composites the behavior suggests that a type-I interface occurs where the hole remains confined entirely within the nanotube and consequently the red-shifts are smaller and almost constant. We conclude that a type-II heterojunction exists between the longer porphyrin oligomers and smaller diameter nanotubes, and this combination provides promise for use in OPVs.

We now consider the strain contribution to the red-shifts, ΔE_{strain}, deduced from eq 2 and shown in Figure 6a for **P6**. The corresponding values for **P2**, **P4**, and **P8** are presented in the Supporting Information (Figure S5). The theory developed by Yang and Han[22] and extended by others[42,43] predicts the nanotube band gap change under small strains to be

$$\Delta E_{\text{strain}} = (\Delta E_{11} - \Delta E_{22})/2 = \left(\frac{2t_0 a_{C-C}}{d}\right)(\varepsilon_\perp - \nu\varepsilon_\parallel) + 3qt_0[(1+\nu)\varepsilon_\parallel \cos 3\theta + \varepsilon_\perp \sin 3\theta] \qquad (3)$$

where t_0 and a_{C-C} are the carbon−carbon transfer integral and bond length, respectively, d is the

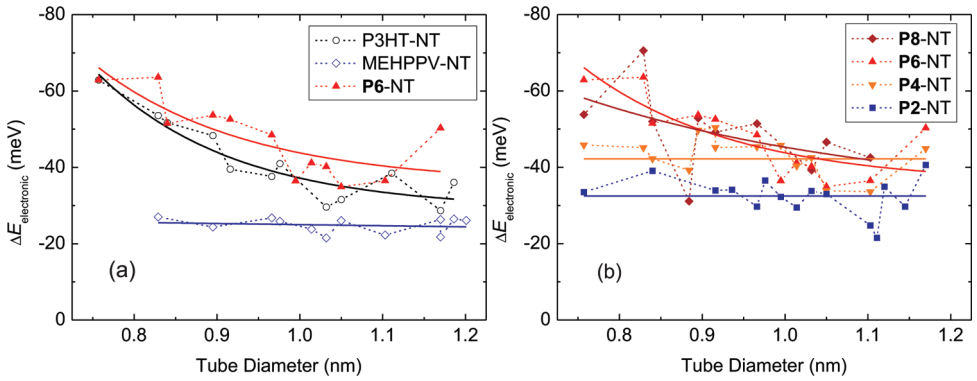

Figure 5. (a) $\Delta E_{electronic}$ components of SWNT red-shifts when in composites with P6, P3HT, and MEHPPV as a function of nanotube diameter. P3HT and MEHPPV data are taken from Schuettfort *et al.*[8] (b) Comparing $\Delta E_{electronic}$ components for the series of oligomers investigated in this study. In both panels a and b, solid lines are fitted exponential decays to act as guides to the eye.

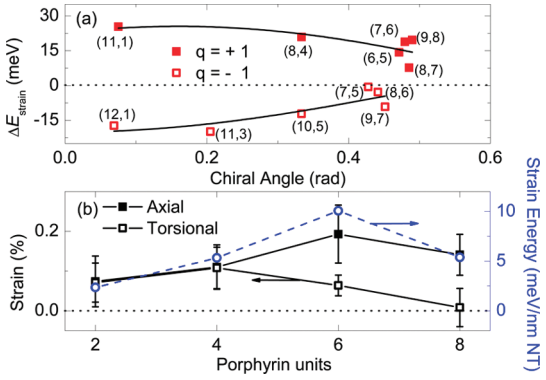

Figure 6. (a) Strain components of red-shifts for P6−SWNT composites. Curves show fits to the data using the Yang and Han model for small strain with the constant term in eq 3 represented by the dotted line. (b) Summary of the axial and torsional strain values obtained for the family of oligomers using the Yang and Han model. Points are mean values of those obtained for the $q = \pm 1$ family for each data set. The total strain energy per unit length of NT is also displayed (see Supporting Information for calculations).

nanotube diameter, ν is Poisson's ratio, and θ is the chiral angle. $\varepsilon_{\parallel}$ and $\varepsilon_{\perp}$ are the strains along the tube axis (uniaxial) and circumference (torsional), respectively, and are used as fitting parameters. The fits use values[27] of $t_0 = 3.0$ eV, $a_{C-C} = 1.432$ Å, and $\nu = 0.20$, with d in the range 0.7−1.2 nm. The solid lines in Figure 6a show fits to this equation for both the $q = +1$ and $q = -1$ families with **P6**, yielding values of $\varepsilon_{\parallel} = 0.19 \pm 0.07\%$ and $\varepsilon_{\perp} = 0.06 \pm 0.03\%$.

Figure 6b shows the two components of SWNT strain obtained for each oligomer together with the total strain energy. The strain energy is largest for **P6** suggesting the strongest binding for this length, consistent with the lower solubility for the extremes of **P2** and **P***N* solutions. The uniaxial component is also proportionately larger for the **P6** and **P8** oligomers, perhaps consistent with the increasing oligomer length which binds along the same axis.

These values are comparable to those found in dried polymer−NT films made from either organic[44] or aqueous solutions[27] and due to differential contraction caused by temperature variation (cooling 260−80 K).[27] However, they have not been previously detected in solution and demonstrate the very strong binding of the porphyrin to the nanotubes. We can calculate the mechanical energy required to induce such a strain in SWNTs from the Young's modulus of the tubes[43] (see Supporting Information for details). The total strain energy is shown as a function of oligomer length in Figure 6b and gives values in the range ~2 to 10 meV/nm NT or ~1 to 4 kJ/mol of porphyrin oligomer with a maximum for **P6**. The dominant contribution to binding is the van der Waals interaction. For a porphyrin monomer, *meso*-5,10,15,20-tetraphenyl (TPP), and NTs this has been estimated, using density functional theory, to be ~80 kJ/mol.[45] For the hexamer, this gives ~500 kJ/mol and is comparable to values calculated elsewhere for polymers of similar length.[46−48] This shows that the strain energy measured in this work is only contributing to a reduction of around 1% of the total binding energy. This component cannot be isolated by other means and is an important parameter in determining the nature of the bonding interaction in these complexes. Our results demonstrate both the sensitivity and power of optical measurements to determine such physical parameters.

We emphasize that no NT strain effects were observed from other semiconducting polymer solutions such as those investigated by Schuettfort *et al.*,[8] namely P3HT and MEHPPV (see Supporting Information Figure S6) and PFO, PIF, and PFB (data not shown). The most energetically favorable configuration for many composites involves the polymer wrapping in a helical manner around the SWNTs.[33,49,50] However, these polymers are much longer but have smaller repeating units when compared to the porphyrin oligomers. The more rigid and larger porphyrin units exceed the nanotube diameters presented here and will tend to lie flat on the nanotube surface as they have been observed to do on gold substrates.[51] Even despite similar planar

configurations,[33] the larger size of the porphyrin units compared to the repeating units of the previously studied conjugated polymers will result in a significantly increased surface area for $\pi-\pi$ interactions. These large $\pi-\pi$ forces will lead to the mechanical strain on the nanotubes, resulting in a predominantly axial deformation of the tube. The significant interaction between the porphyrin oligomers and nanotubes is consistent with the extremely high binding constants for formation of these complexes.[20]

CONCLUSION

We have investigated the binding of porphyrin oligomers to SWNTs and made two remarkable observations. First, the binding of porphyrin oligomers to SWNTs is so strong that it induces mechanical strain on the nanotubes, even in solution. Strain values of this magnitude have only been observed previously in the solid state.[27,44] This effect is not observed for any of the other semiconducting polymers investigated here and appears to be unique to the porphyrin oligomers. These findings are consistent with the large binding constants deduced in our previous work.[20] Second, a type-II heterojunction exists between the longer porphyrin oligomers (**P6**, **P8** and **P***N*) and smaller-diameter SWNTs. The type-II interface causes a strong red-shifted absorption and emission of the nanotubes when small nanotubes are dispersed with porphyrin oligomers. This effect disappears for larger diameter nanotubes or shorter oligomers (*e.g.,* **P2**) where no type-II interface is expected. This is attributed to an exciton state where the wave function of the SWNT hole extends across the interface due to the band alignment, effectively lowering the energy of the exciton. These results provide a promising avenue for incorporating porphyrin−SWNT composites in efficient OPVs, utilizing the mobilities of both materials and the broad absorption bands of the porphyrin oligomers to capture a wide range of the solar spectrum.

MATERIALS AND METHODS

Synthetic Procedures. Porphyrin oligomers **P2**,[34] **P4**,[34] **P6**,[40] **P8**,[52] and **P***N*[11] were synthesized according to published procedures. Purified HiPCO SWNTs were purchased from Carbon Nanotechnologies, Inc. (CNI) and SG65 CoMoCAT SWNTs from SouthWest NanoTechnologies (SWeNT), and both types were used without further treatment. In a typical experiment, 2 mg of porphyrin and 1 mg of SWNT were sonicated for 1 h in 4 mL of tetrahydrofuran (THF) using a Branson 1510E-MT sonicator bath (80 W, 40 kHz) cooled with ice. The resulting dark solution was centrifuged for 1.5 h at 4800 rpm and passed over glass wool to remove insoluble carbonaceous residues. The porphyrin nanotube complex was isolated with a microfilter (nylon, pore size 200 nm) and then washed with THF until the excess porphyrin was removed and the filtrate was colorless. To redisperse the nanotubes in solvent, the nylon membrane with the nanotube film was sonicated for a few seconds in 2 mL of THF using an ultrasonic bath. Generally, HiPCO solutions were more stable than CoMoCAT solutions while **P***N*−CoMoCAT solutions and all **P2** solutions required a large excess of oligomer to prevent significant nanotube aggregation.

Sodium dodecylbenzene sulfonate (SDBS)-wrapped nanotubes were prepared by dissolving 15 mg of SWNT material and 350 mg of SDBS in 35 mL of D_2O. The mixture was treated in an ultrasonic disintegrator for 30 min, followed by ultracentrifugation at 100000*g* for 4 h.

Spectroscopy. All absorption measurements were carried out using a Perkin-Elmer Lambda 9 UV−vis−NIR Spectrophotometer. PLE mapping was carried out using a custom-built setup described elsewhere.[6] Briefly, a 75 W xenon lamp is focused into a monochromator to illuminate the sample in a quartz fluorescence cuvette. A broad excitation wavelength range (350−1000 nm) is achieved and a silicon photodiode is used to normalize for the excitation intensity. The PL from the sample is collected at 90° to the excitation axis and focused onto a spectrograph fitted with a liquid nitrogen cooled InGaAs photodiode array. The detector's spectral response function was obtained using a standard tungsten lamp and used to correct the spectra. Appropriate filters were used on both the excitation and detection ends to remove unwanted wavelengths.

Acknowledgment. The authors thank the Engineering and Physical Sciences Research Council and the European Commission (EU Contract MRTN-CT-2006-036040) for their financial support. S. Stranks acknowledges the Rhodes Trust for financial support.

Supporting Information Available: Figures showing all absorption spectra, PLE maps, red-shifts, and strains of the SWNT−porphyrin oligomer composites and calculations of the oligomer energy levels and strain values. This material is available free of charge *via* the Internet at http://pubs.acs.org.

REFERENCES AND NOTES

1. Chen, H. Y.; Hou, J. H.; Zhang, S. Q.; Liang, Y. Y.; Yang, G. W.; Yang, Y.; Yu, L. P.; Wu, Y.; Li, G. Polymer Solar Cells with Enhanced Open-Circuit Voltage and Efficiency. *Nat. Photonics* **2009,** *3*, 649–653.
2. Green, M. A.; Emery, K.; Hishikawa, Y.; Warta, W. Solar Cell Efficiency Tables (version 36). *Prog. Photovoltaics* **2010,** *18*, 346–352.
3. Tang, C. W. Two-Layer Organic Photovoltaic Cell. *Appl. Phys. Lett.* **1986,** *48*, 183–185.
4. Reich, S.; Thomsen, C.; Maultzsch, J. *Carbon Nanotubes−Basic Concepts and Physical Properties*, 1st ed.; Wiley-VCH: New York, 2004.
5. Schuettfort, T.; Snaith, H. J.; Nish, A.; Nicholas, R. J. Synthesis and Spectroscopic Characterization of Solution Processable Highly Ordered Polythiophene-Carbon Nanotube Nanohybrid Structures. *Nanotechnology* **2010,** *21*, 025201.
6. Nish, A.; Hwang, J. Y.; Doig, J.; Nicholas, R. J. Direct Spectroscopic Evidence of Energy Transfer from Photoexcited Semiconducting Polymers to Single-Walled Carbon Nanotubes. *Nanotechnology* **2008,** *19*, 095603.
7. Kanai, Y.; Grossman, J. C. Role of Semiconducting and Metallic Tubes in P3HT/Carbon−Nanotube Photovoltaic Heterojunctions: Density Functional Theory Calculations. *Nano Lett.* **2008,** *8*, 908–912.
8. Schuettfort, T.; Nish, A.; Nicholas, R. J. Observation of a Type II Heterojunction in a Highly Ordered Polymer−Carbon Nanotube Nanohybrid Structure. *Nano Lett.* **2009,** *9*, 3871–3876.
9. Stranks, S. D.; Weisspfennig, C.; Parkinson, P.; Johnston, M. B.; Herz, L. M.; Nicholas, R. J. Ultrafast Charge Separation at a Polymer−Single-Walled Carbon Nanotube Molecular Junction. *Nano Lett.* **2011,** *11*, 66–72.

10. Pullerits, T.; Sundström, V. Photosynthetic Light-Harvesting Pigment−Protein Complexes: Toward Understanding How and Why. *Acc. Chem. Res.* **1996,** *29*, 381–389.
11. Grozema, F. C.; Houarner-rassin, C.; Prins, P.; Siebbeles, L. D. A.; Anderson, H. L. Supramolecular Control of Charge Transport in Molecular Wires. *J. Am. Chem. Soc.* **2007,** *129*, 13370–13371.
12. Sedghi, G.; Sawada, K.; Esdaile, L. J.; Hoffmann, M.; Anderson, H. L.; Bethell, D.; Haiss, W.; Higgins, S. J.; Nichols, R. J. Single Molecule Conductance of Porphyrin Wires with Ultralow Attenuation. *J. Am. Chem. Soc.* **2008,** *130*, 8582–8583.
13. Sirringhaus, H.; Tessler, N.; Friend, R. H. Integrated Optoelectronic Devices Based on Conjugated Polymers. *Science* **1998,** *280*, 1741–1744.
14. Cheng, F. Y.; Adronov, A. Noncovalent Functionalization and Solubilization of Carbon Nanotubes by Using a Conjugated Zn−Porphyrin Polymer. *Chem.—Eur. J.* **2006,** *12*, 5053–5059.
15. Li, H. P.; Zhou, B.; Lin, Y.; Gu, L. R.; Wang, W.; Fernando, K. A. S.; Kumar, S.; Allard, L. F.; Sun, Y. P. Selective Interactions of Porphyrins with Semiconducting Single-Walled Carbon Nanotubes. *J. Am. Chem. Soc.* **2004,** *126*, 1014–1015.
16. Casey, J. P.; Bachilo, S. M.; Weisman, R. B. Efficient Photosensitized Energy Transfer and Near-IR Fluorescence from Porphyrin−SWNT Complexes. *J. Mater. Chem.* **2008,** *18*, 1510–1516.
17. Magadur, G.; Lauret, J. S.; Alain-rizzo, V.; Voisin, C.; Roussignol, P.; Deleporte, E.; Delaire, J. A. Excitation Transfer in Functionalized Carbon Nanotubes. *ChemPhysChem* **2008,** *9*, 1250–1253.
18. Roquelet, C.; Lauret, J. S.; Alain-rizzo, V.; Voisin, C.; Fleurier, R.; Delarue, M.; Garrot, D.; Loiseau, A.; Roussignol, P.; Delaire, J. A.; *et al.* π-Stacking Functionalization of Carbon Nanotubes through Micelle Swelling. *ChemPhysChem* **2010,** *11*, 1667–1672.
19. Cheng, F. Y.; Zhang, S.; Adronov, A.; Echegoyen, L.; Diederich, F. Triply Fused Zn(II)−Porphyrin Oligomers: Synthesis, Properties, and Supramolecular Interactions with Single-Walled Carbon Nanotubes (SWNTs). *Chem.—Eur. J.* **2006,** *12*, 6062–6070.
20. Sprafke, J. K.; Stranks, S. D.; Warner, J. H.; Nicholas, R. J.; Anderson, H. L. Noncovalent Binding of Carbon Nanotubes by Porphyrin Oligomers. *Angew. Chem., Int. Ed.* 2011, *50*, 2313−2316.
21. Yang, L.; Anantram, M. P.; Han, J.; Lu, J. P. Band-Gap Change of Carbon Nanotubes: Effect of Small Uniaxial and Torsional Strain. *Phys. Rev. B* **1999,** *60*, 13874–13878.
22. Yang, L.; Han, J. Electronic Structure of Deformed Carbon Nanotubes. *Phys. Rev. Lett.* **2000,** *85*, 154–157.
23. Deacon, R. S.; Chuang, K. C.; Doig, J.; Mortimer, I. B.; Nicholas, R. J. Photoluminescence Study of Aqueous-Surfactant-Wrapped Single-Walled Carbon Nanotubes under Hydrostatic Pressure. *Phys. Rev. B* **2006,** *74*, 201402.
24. Arnold, K.; Lebedkin, S.; Kiowski, O.; Hennrich, F.; Kappes, M. M. Matrix-Imposed Stress-Induced Shifts in the Photoluminescence of Single-Walled Carbon Nanotubes at Low Temperatures. *Nano Lett.* **2004,** *4*, 2349–2354.
25. Leeuw, T. K.; Tsyboulski, D. A.; Nikolaev, P. N.; Bachilo, S. M.; Arepalli, S.; Weisman, R. B. Strain Measurements on Individual Single-Walled Carbon Nanotubes in a Polymer Host: Structure-Dependent Spectral Shifts and Load Transfer. *Nano Lett.* **2008,** *8*, 826–831.
26. Huang, M. Y.; Wu, Y.; Chandra, B.; Yan, H.; Shan, Y.; Heinz, T. F.; Hone, J. Direct Measurement of Strain-Induced Changes in the Band Structure of Carbon Nanotubes. *Phys. Rev. Lett.* **2008,** *100*, 136803.
27. Li, L. J.; Nicholas, R. J.; Deacon, R. S.; Shields, P. A. Chirality Assignment of Single-Walled Carbon Nanotubes with Strain. *Phys. Rev. Lett.* **2004,** *93*, 156104.
28. Anderson, H. L. Conjugated Porphyrin Ladders. *Inorg. Chem.* **1994,** *33*, 972–981.
29. Winters, M. U.; Kärnbratt, J.; Eng, M.; Wilson, C. J.; Anderson, H. L.; Albinsson, B. Photophysics of a Butadiyne-Linked Porphyrin Dimer: Influence of Conformational Flexibility in the Ground and First Singlet Excited State. *J. Phys. Chem. C* **2007,** *111*, 7192–7199.
30. Taylor, P. N.; Huuskonen, J.; Rumbles, G.; Aplin, R. T.; Williams, E.; Anderson, H. L. Conjugated Porphyrin Oligomers from Monomer to Hexamer. *Chem. Commun.* **1998,** 909–910.
31. Chang, M. H.; Hoffmann, M.; Anderson, H. L.; Herz, L. M. Dynamics of Excited-State Conformational Relaxation and Electronic Delocalization in Conjugated Porphyrin Oligomers. *J. Am. Chem. Soc.* **2008,** *130*, 10171–10178.
32. Beljonne, D.; OKeefe, G. E.; Hamer, P. J.; Friend, R. H.; Anderson, H. L.; Brédas, J. L. Investigation of the Linear and Nonlinear Optical Response of Edge-Linked Conjugated Zinc Porphyrin Oligomers by Optical Spectroscopy and Configuration Interaction Techniques. *J. Chem. Phys.* **1997,** *106*, 9439–9460.
33. Bernardi, M.; Giulianini, M.; Grossman, J. C. Self-Assembly and Its Impact on Interfacial Charge Transfer in Carbon Nanotube/P3HT Solar Cells. *ACS Nano* **2010,** *4*, 6599–6606.
34. Winters, M. U.; Dahlstedt, E.; Blades, H. E.; Wilson, C. J.; Frampton, M. J.; Anderson, H. L.; Albinsson, B. Probing the Efficiency of Electron Transfer through Porphyrin-Based Molecular Wires. *J. Am. Chem. Soc.* **2007,** *129*, 4291–4297.
35. D'Andrade, B. W.; Datta, S.; Forrest, S. R.; Djurovich, P.; Polikarpov, E.; Thompson, M. E. Relationship Between the Ionization and Oxidation Potentials of Molecular Organic Semiconductors. *Org. Electron.* **2005,** *6*, 11–20.
36. Kuimova, M. K.; Hoffmann, M.; Winters, M. U.; Eng, M.; Balaz, M.; Clark, I. P.; Collins, H. A.; Tavender, S. M.; Wilson, C. J.; Albinsson, B.; *et al.* Determination of the Triplet State Energies of a Series of Conjugated Porphyrin Oligomers. *Photochem. Photobiol. Sci.* **2007,** *6*, 675–682.
37. Weisman, R. B.; Bachilo, S. M. Dependence of Optical Transition Energies on Structure for Single-Walled Carbon Nanotubes in Aqueous Suspension: an Empirical Kataura Plot. *Nano Lett.* **2003,** *3*, 1235–1238.
38. Reich, S.; Thomsen, C.; Robertson, J. Exciton Resonances Quench the Photoluminescence of Zigzag Carbon Nanotubes. *Phys. Rev. Lett.* **2005,** *95*, 077402.
39. Oyama, Y.; Saito, R.; Sato, K.; Jiang, J.; Samsonidze, G. G.; Gruneis, A.; Miyauchi, Y.; Maruyama, S.; Jorio, A.; Dresselhaus, G.; *et al.* Photoluminescence Intensity of Single-Wall Carbon Nanotubes. *Carbon* **2006,** *44*, 873–879.
40. Hoffmann, M.; Kärnbratt, J.; Chang, M. H.; Herz, L. M.; Albinsson, B.; Anderson, H. L. Enhanced p-Conjugation around a Porphyrin [6] Nanoring. *Angew. Chem., Int. Ed.* **2008,** *120*, 5071–5074.
41. Chuang, K. C.; Nish, A.; Hwang, J. Y.; Evans, G. W.; Nicholas, R. J. Experimental Study of Coulomb Corrections and Single-Particle Energies for Single-Walled Carbon Nanotubes Using Cross-Polarized Photoluminescence. *Phys. Rev. B* **2008,** *78*, 085411.
42. Gartstein, Y. N.; Zakhidov, A. A.; Baughman, R. H. Mechanical and Electromechanical Coupling in Carbon Nanotube Distortions. *Phys. Rev. B* **2003,** *68*, 115415.
43. Capaz, R. B.; Spataru, C. D.; Tangney, P.; Cohen, M. L.; Louie, S. G. Hydrostatic Pressure Effects on the Structural and Electronic Properties of Carbon Nanotubes. *Phys. Status Solidi B* **2004,** *241*, 3352–3359.
44. Nish, A.; Nicholas, R. J.; Faugeras, C.; Bao, Z.; Potemski, M. High-Field Magnetooptical Behavior of Polymer-Embedded Single-Walled Carbon Nanotubes. *Phys. Rev. B* **2008,** *78*, 245413.
45. Karachevtsev, V. A.; Zarudnev, E. S.; Stepanian, S. G.; Glamazda, A. Y.; Karachevtsev, M. V.; Adamowicz, L. Raman Spectroscopy and Theoretical Characterization of Nanohybrids of Porphyrins with Carbon Nanotubes. *J. Phys. Chem. C* **2010,** *114*, 16215–16222.
46. Tallury, S. S.; Pasquinelli, M. A. Molecular Dynamics Simulations of Polymers with Stiff Backbones Interacting with Single-Walled Carbon Nanotubes. *J. Phys. Chem. B* **2010,** *114*, 9349–9355.

47. Tallury, S. S.; Pasquinelli, M. A. Molecular Dynamics Simulations of Flexible Polymer Chains Wrapping Single-Walled Carbon Nanotubes. *J. Phys. Chem. B* **2010,** *114*, 4122–4129.
48. Panhuis, M. I. H.; Maiti, A.; Dalton, A. B.; Coleman, J. N.; McCarthy, B.; Blau, W. J. Selective Interaction in a Polymer-Single-Wall Carbon Nanotube Composite. *J. Phys. Chem. B* **2003,** *107*, 478–482.
49. Giulianini, M.; Waclawik, E. R.; Bell, J. M.; Castrucci, P.; Scarselli, M.; Motta, N. Regioregular Poly(3-hexylthiophene) Helical Self-Organization on Carbon Nanotubes. *Appl. Phys. Lett.* **2009,** *95*, 013304.
50. Hwang, J. Y.; Nish, A.; Doig, J.; Douven, S.; Chen, C.-W.; Chen, L. C.; Nicholas, R. J. Polymer Structure and Solvent Effects on the Selective Dispersion of Single-Walled Carbon Nanotubes. *J. Am. Chem. Soc.* **2008,** *130*, 3543–3553.
51. Saywell, A.; Sprafke, J. K.; Esdaile, L. J.; Britton, A. J.; Rienzo, A.; Anderson, H. L.; O'Shea, J. N.; Beton, P. Conformation and Packing of Porphyrin Polymer Chains Deposited Using Electrospray on a Gold Surface. *Angew. Chem., Int. Ed.* **2010,** *49*, 9136–9139.
52. Drobizhev, M.; Stepanenko, Y.; Rebane, A.; Wilson, C. J.; Screen, T. E. O.; Anderson, H. L. Strong Cooperative Enhancement of Two-Photon Absorption in Double-Strand Conjugated Porphyrin Ladder Arrays. *J. Am. Chem. Soc.* **2006,** *128*, 12432–12433.